Fourth-generation-quark production at the Superconducting Super Collider

Sally Dawson
Physics Department, Brookhaven National Laboratory, Upton, New York 11973

Stephen Godfrey
Guelph-Waterloo Program for Graduate Work in Physics, Department of Physics, University of Guelph, Guelph, Canada N1G 2W1

(Received 10 June 1988)

The production of fourth-generation quarks at the Superconducting Super Collider is studied concentrating on event signatures resulting from the single-lepton and two-lepton decay modes. We find that events with multijets ($n_{\rm jet} \geq 3$) and one or two high-p_T leptons are good signals for heavy-quark production for quark masses up to 600 GeV. In addition, we also found that the total transverse energy of an event is useful for distinguishing between heavy-quark production and the top-quark background.

I. INTRODUCTION

High-energy hadron colliders provide a window for probing many types of new physics.[1] One interesting question which these machines can address is whether the proliferation of families extends beyond three generations. The proposed Superconducting Super Collider (SSC) will extend our knowledge of heavy quarks up to mass scales on the order of 600 GeV. In this paper we study the experimental signatures of a possible fourth generation of heavy quarks and we present extensive numerical results for pp collisions at $\sqrt{s}=40$ TeV. Our goal is to find signatures of heavy-quark production that can be differentiated from conventional physics backgrounds. It is important that the ability to detect fourth-generation quarks be clearly demonstrated since a fourth generation is one of the most straightforward extensions of the standard model and hence a benchmark test of the capabilities of any new machine.

Very few restrictions exist on the masses of fourth-generation quarks. Measurements of the ρ parameter require[2]

$$|M_U - M_D| < 180 \text{ GeV} , \tag{1.1}$$

if the standard model is to be consistent. [We call the charge $\frac{2}{3}$ ($-\frac{1}{3}$) member of the $SU(2)_L$ quark doublet U (D).] This argument does not restrict the magnitude of the mass scale, however. The ρ-parameter limit can also be interpreted as a limit on the heavy-quark lifetime. If $M_U, M_D \gg M_W$, then[9]

$$\sum_j |V_{jD}|^2 \left[\frac{M_D}{M_W}\right]^2 < 5, \quad \sum_j |V_{Uj}|^2 \left[\frac{M_U}{M_W}\right]^2 < 5 , \tag{1.2}$$

where V_{ij} are the elements of the 4×4 Kobayashi-Maskawa (KM) mixing matrix. This translates into the limit on the heavy-D-quark lifetime,

$$\tau > 5\times10^{-26}\left[\frac{1 \text{ TeV}}{M_D}\right] \text{ sec} . \tag{1.3}$$

Unitarity considerations[4] imply that if a quark is heavier than about 500 GeV then the quark is strongly interacting and perturbation theory is no longer valid. This is not an argument against the existence of heavier-mass quarks; it merely says that we cannot calculate their production cross sections reliably. To be conservative we will present results for $M_Q < 600$ GeV.

By analogy with the third generation of quarks we assume $M_U \gg M_D$ and consider only the production of the D quark. If M_U is comparable to M_D, then there is an additional source of D quarks from the decay

$$U \rightarrow W^+ D . \tag{1.4}$$

Our results are therefore conservative estimates of the production rates. The D quark decays weakly via the real or virtual emission of a W boson and so its decay rates are governed by the 4×4 KM matrix. We assume that the KM matrix is approximately diagonal.

The signal for the decay of the D quark is jets plus some number of leptons. For $M_D > M_W + M_t$, the D quark decays primarily to a $W^- t$ pair. Pair production of D quarks thus yields final states with $W^+W^-t\bar{t}$. We consider both the case where the top quark is lighter than the W boson ($M_t = 50$ GeV) and where it is heavier ($M_t = 100$ GeV). If the top quark is heavier than the W boson then it will decay to $W^+ b$ and D-quark pair production will result in a final state with four W's and a $b\bar{b}$ pair. On the other hand, if the t quark is lighter than the W boson it will decay to a b quark plus either $l\bar{\nu}$ or a lighter $q\bar{q}$ pair with a relatively soft momentum spectrum. Thus, the signals for D-quark production are quite different for $M_t < M_W$ and for $M_t > M_W$. Here, we do not discuss top-quark production alone, but consider it merely as a background for fourth-generation-quark production.[5]

In this paper we discuss both the one- and two-lepton plus multijet signals for heavy-quark production. We do not include the multilepton ($n_l > 2$) plus jet signals since they have been discussed previously by many authors.[6-8] In Secs. II and III we consider the one-lepton signal for $M_t = 50$ GeV and 100 GeV, respectively, and in Secs. IV and V we discuss the two-lepton signal. In Sec. VI we present our conclusions and mention some unanswered questions.

II. ONE-LEPTON SIGNAL ($M_t = 50$ GeV)

In this section we consider $D\bar{D}$ pair production where the final state is one high-p_T lepton plus jets. We compare this signal with the background from $t\bar{t}$ production for $M_t = 50$ GeV. In this case, the top quark cannot decay into a physical W and there are two possible decay chains for the $D\bar{D}$ which lead to a single lepton in the final state (see Fig. 1). In determining the branching ratios and the background we have assumed that the sign of the lepton can be distinguished. All of our figures for the one lepton scenario are summed over $e^{\pm}$ and $\mu^{\pm}$ production. The Eichten-Hinchliffe-Lane-Quigg[1] (EHLQ) structure functions with $\Lambda_{QCD} = 200$ MeV are used everywhere with the structure functions evaluated at the scale $\mu = M_D$. All of our results are for pp collisions at $\sqrt{s} = 40$ TeV.

For $M_D > 100$ GeV, D-quark pair production occurs predominantly through the hard parton interactions, $q\bar{q} \to Q\bar{Q}$ and $gg \to Q\bar{Q}$. The tree-level cross sections have been known for some time and we do not reproduce them here.[9] The total cross section for heavy-quark pair production is shown in Fig. 2 for pp collisions at $\sqrt{s} = 40$ TeV and is quite large. In obtaining our results we have used the lowest-order cross section with the one-loop value for α_s, where we have taken the renormalization scale to be M_D. The $O(\alpha_s^3)$ corrections to heavy-quark production have recently been calculated and tend to increase the cross section.[10] Our results can hence be considered as lower bounds on the production rates.

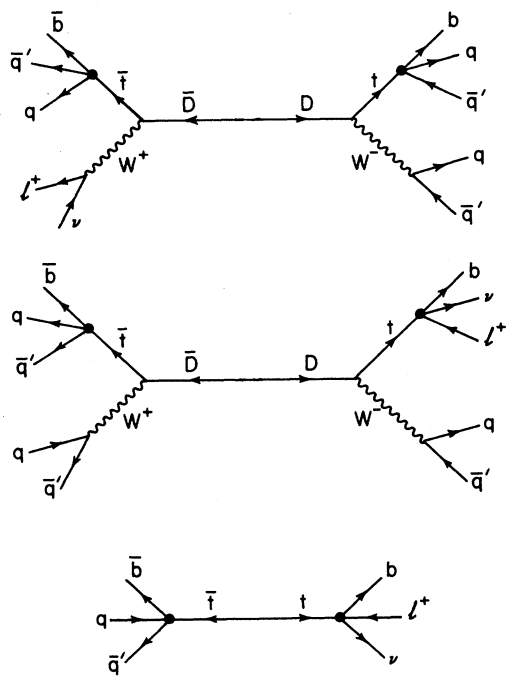

FIG. 1. Decay chains leading to a single lepton in the final state when $M_t = 50$ GeV. Also shown is the background from $t\bar{t}$ production.

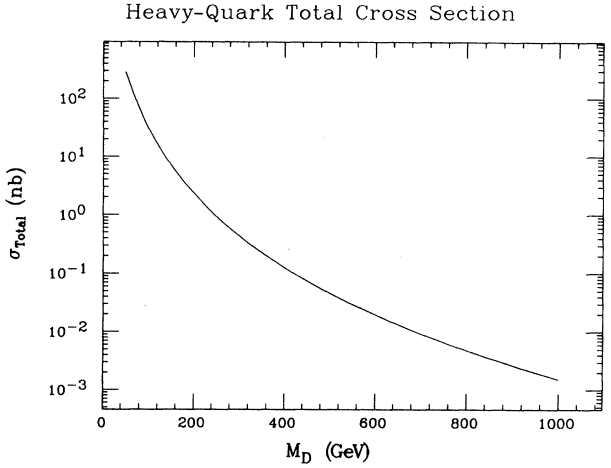

FIG. 2. Total cross section for $pp \to D\bar{D}$ at $\sqrt{s} = 40$ TeV. This cross section includes no branching ratios.

Our results are generated using a simple parton model Monte Carlo with no hadronization. (We used 500 000 Monte Carlo points to obtain each curve. The slight waviness of some of the curves is due to statistical fluctuations.) For several distributions we have compared our results with those obtained from ISAJET[11] (which includes hadronization) and found good agreement. Hence, we expect that hadronization will not greatly affect our conclusions. In addition, the b quark has been treated as a hadronic jet since its decay will not yield high-p_T leptons. With our jet-finding algorithm (described below) the quarks resulting from the decay of a b quark always coalesce into a single jet.

The cross sections for D-quark production and decay via the chain of Fig. 1 are given in Table I. Since these cross sections are large, relatively stringent cuts may be applied to extract the signal, as we shall see.

We examined numerous distributions of kinematic variables. In what follows we show those which most successfully distinguish between the $D\bar{D}$ signal and the $t\bar{t}$ background. We begin by showing some simple kinematic variables for $D\bar{D}$ and $t\bar{t}$ pair production. All of our figures for the D signal and the t background are summed over all the possible decay chains. We define the variables

$$E_T \equiv \sum_{\text{visible energy}} \sqrt{p_{1i}^2 + p_{2i}^2} ,$$
$$\mathcal{M}_T(p_l, p_T^{\text{miss}}) \equiv \sqrt{p_{1T} p_T^{\text{miss}} (1 - \cos\theta_T)} , \tag{2.1}$$
$$P_T(p_l, p_T^{\text{miss}}) \equiv p_{1T} \sin\theta_T ,$$

where p_3 is the beam direction, θ_T is the angle separating the lepton and missing momentum in the plane transverse to the beam direction, p_{lT} is the transverse momentum of the lepton, and p_T^{miss} is the total missing transverse energy.

In Figs. 3, 4, 5, and 6, we show the p_T spectrum of the lepton, E_T, the total transverse energy of the process, $\mathcal{M}_T(p_l, p_T^{\text{miss}})$, the invariant mass in the transverse plane of the lepton and the missing transverse momentum, and

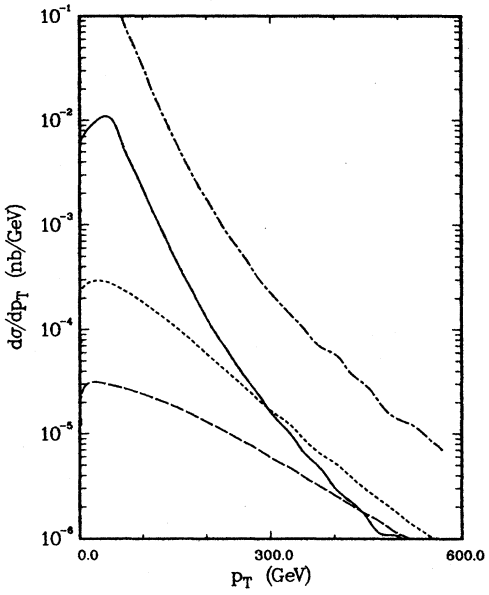

FIG. 3. p_T distribution of the final lepton for the one-lepton decay chain of Fig. 1 for $M_t = 50$ GeV for $pp \to D\bar{D}$ at $\sqrt{s} = 40$ GeV. The dot-dash line is the background from $t\bar{t}$ production and the solid, dotted, and dashed lines are the $D\bar{D}$ signal with $M_D = 200$, 400, and 600 GeV, respectively.

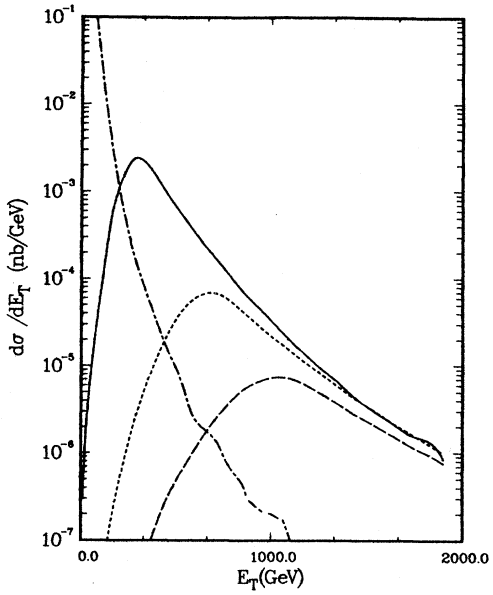

FIG. 4. E_T distribution for the one-lepton decay chain of Fig. 1 for $M_t = 50$ GeV for $pp \to D\bar{D}$ at $\sqrt{s} = 40$ TeV. The dot-dash line is the background from $t\bar{t}$ production and the solid, dotted, and dashed lines are the $D\bar{D}$ signal with $M_D = 200$, 400, and 600 GeV, respectively.

TABLE I. $D\bar{D} \to 1$ lepton plus jets ($M_t = 50$ GeV). σ is the cross section for $pp \to D\bar{D} \to l^{\pm}X$ at $\sqrt{s} = 40$ TeV and $l = e$ or μ. σ^{A} has $E_T > 800$ GeV, σ^{B} has $\mathcal{M}_T(p_l, p_T^{\mathrm{miss}}) > 50$ GeV, σ^{C} has $P_T(p_l, p_T^{\mathrm{miss}}) > 150$ GeV, and σ^{D} has all three of the previous cuts. The column labeled $t\bar{t}$ is the background from $pp \to t\bar{t}$. All cross sections are in nb.

	$M_D = 200$ GeV	$M_D = 400$ GeV	$M_D = 600$ GeV	$t\bar{t}$
σ	0.64	3.3×10^{-2}	5.2×10^{-3}	1.1×10^{2}
σ^{A}	1.9×10^{-2}	1.3×10^{-2}	4.6×10^{-3}	1.0×10^{-4}
σ^{B}	0.16	8.1×10^{-3}	1.3×10^{-3}	
σ^{C}	2.1×10^{-3}	4.4×10^{-4}	1.3×10^{-4}	2.0×10^{-5}
σ^{D}	1.5×10^{-4}	1.4×10^{-4}	9.0×10^{-5}	
$\sigma_{1\text{ jet}}$	6.4×10^{-3}	1.7×10^{-5}	1.1×10^{-6}	5.1×10^{1}
$\sigma^{\mathrm{A}}_{1\text{ jet}}$	1.9×10^{-7}	8.1×10^{-6}	4.9×10^{-7}	1.2×10^{-5}
$\sigma^{\mathrm{B}}_{1\text{ jet}}$	3.3×10^{-3}	7.1×10^{-6}	4.7×10^{-7}	
$\sigma^{\mathrm{C}}_{1\text{ jet}}$	3.0×10^{-4}	7.3×10^{-7}	3.2×10^{-8}	
$\sigma^{\mathrm{D}}_{1\text{ jet}}$		7.3×10^{-7}		
$\sigma_{2\text{ jet}}$	1.2×10^{-1}	3.0×10^{-3}	4.4×10^{-4}	2.5×10^{1}
$\sigma^{\mathrm{A}}_{2\text{ jet}}$	1.3×10^{-2}	1.1×10^{-3}	3.6×10^{-4}	9.0×10^{-5}
$\sigma^{\mathrm{B}}_{2\text{ jet}}$	3.9×10^{-2}	1.1×10^{-3}	1.7×10^{-4}	
$\sigma^{\mathrm{C}}_{2\text{ jet}}$	1.0×10^{-3}	6.9×10^{-5}	2.0×10^{-5}	2.0×10^{-5}
$\sigma^{\mathrm{D}}_{2\text{ jet}}$	1.5×10^{-4}	1.7×10^{-5}	1.3×10^{-5}	
$\sigma_{3\text{ jet}}$	2.6×10^{-1}	1.6×10^{-2}	2.8×10^{-3}	1.24
$\sigma^{\mathrm{A}}_{3\text{ jet}}$	5.7×10^{-3}	6.1×10^{-3}	2.5×10^{-3}	
$\sigma^{\mathrm{B}}_{3\text{ jet}}$	7.5×10^{-2}	5.5×10^{-3}	1.0×10^{-3}	
$\sigma^{\mathrm{C}}_{3\text{ jet}}$	5.9×10^{-4}	3.1×10^{-4}	9.6×10^{-4}	
$\sigma^{\mathrm{D}}_{3\text{ jet}}$	5.3×10^{-7}	1.1×10^{-4}	7.3×10^{-5}	
$\sigma_{4\text{ jet}}$	2.0×10^{-1}	1.1×10^{-2}	1.7×10^{-3}	
$\sigma^{\mathrm{A}}_{4\text{ jet}}$	5.7×10^{-4}	4.3×10^{-3}	1.5×10^{-3}	
$\sigma^{\mathrm{B}}_{4\text{ jet}}$	3.7×10^{-2}	1.44×10^{-3}	1.4×10^{-4}	
$\sigma^{\mathrm{C}}_{4\text{ jet}}$	1.9×10^{-4}	5.3×10^{-5}	9.3×10^{-6}	
$\sigma^{\mathrm{D}}_{4\text{ jet}}$		1.5×10^{-5}	5.7×10^{-6}	

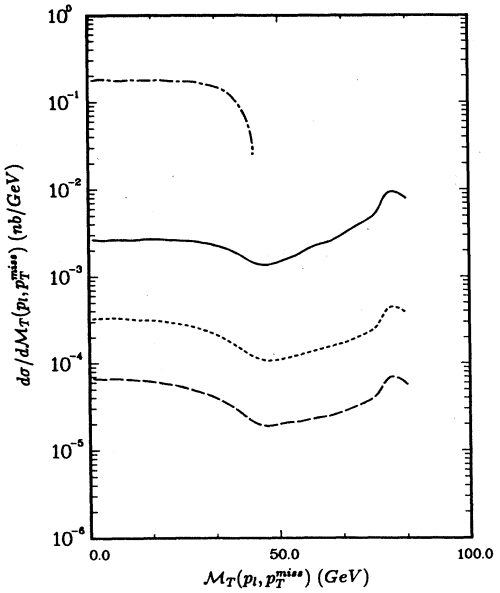

FIG. 5. Invariant mass in the transverse plane of the lepton and the missing transverse momentum $\mathcal{M}_T(p_l,p_T^{\rm miss})$ for the one-lepton decay chain of Fig. 1 for $M_t=50$ GeV for $pp\to D\bar{D}$ at $\sqrt{s}=40$ TeV. The dot-dash line is the background from $t\bar{t}$ production and the solid, dotted, and dashed lines are the $D\bar{D}$ signal with $M_D=200$, 400, and 600 GeV, respectively.

$P_T(p_{1T},p_T^{\rm miss})$, the transverse momentum between the lepton and the missing p_T. The p_T signal from the lepton looks similar for the $D\bar{D}$ signal and the $t\bar{t}$ background and extends out to p_T on the order of 600 GeV. The p_T signal peaks near the t-quark mass. Note the abrupt cutoff in Fig. 5 at $\mathcal{M}_T=M_W$ for the heavy-quark signal and the cutoff at $\mathcal{M}_T=M_t$ for the top-quark background.

The E_T, $\mathcal{M}_T(p_l,p_T^{\rm miss})$, and $P_T(p_l,p_T^{\rm miss})$ signals all behave quite differently for the top quark and the $D\bar{D}$ signal. Hence cuts on any of these variables will be efficient in rejecting the top-quark background. This is illustrated in Table I, where the effect of various cuts are shown.

The series of cuts

$$E_T>800\ \text{GeV}\ ,$$
$$P_T(p_l,p_T^{\rm miss})>150\ \text{GeV}\ , \tag{2.2}$$
$$\mathcal{M}_T(p_l,p_T^{\rm miss})>50\ \text{GeV}$$

cleanly rejects the top-quark background, as can be seen from Table I. The D-quark cross section with these cuts is relatively insensitive to the quark mass and is about 0.1 pb at $\sqrt{s}=40$ TeV, which corresponds to 1000 events per year with an integrated luminosity of $10^{40}/\text{cm}^2$.

An alternate technique for identifying heavy quarks is to look for multijets plus a single isolated lepton. Our jets are defined such that they have $p_T>30$ GeV and $\Delta R\equiv(\Delta\phi^2+\Delta\eta^2)^{1/2}>1$, where $\Delta\phi$ is the azimuthal separation between jets and $\Delta\eta$ is the rapidity gap. If two quarks have $\Delta R<1$, then they are coalesced into a single jet. The one-, two-, three-, and four-jet cross sections are shown in Fig. 7 as a function of the heavy-quark mass for the decay chain of Fig. 1. The two-, three-, and four-jet cross sections are large for the D quark, while top-quark production tends to yield events with less than three jets. From Table I, we see that the four-jet cross section has no background from $t\bar{t}$ production. Combinations of cuts on E_T, $P_T(p_l,p_T^{\rm miss})$, and $\mathcal{M}_T(p_l,p_T^{\rm miss})$ and two- or three-

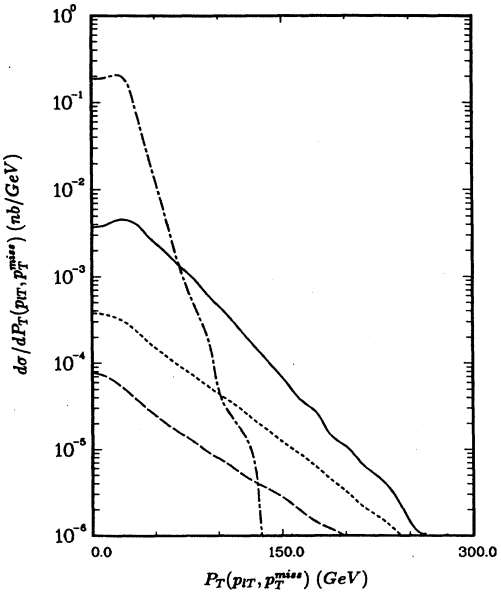

FIG. 6. Transverse momentum between the lepton and the missing transverse momentum $P_T(p_l,p_T^{\rm miss})$ for the one-lepton decay chain of Fig. 1 for $M_t=50$ GeV for $pp\to D\bar{D}$ at $\sqrt{s}=40$ TeV. The dot-dash line is the background from $t\bar{t}$ production and the solid, dotted, and dashed lines are the $D\bar{D}$ signal with $M_D=200$, 400, and 600 GeV, respectively.

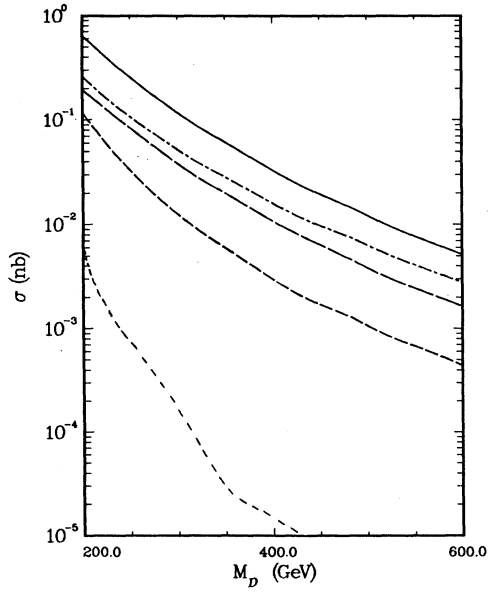

FIG. 7. Multijet cross sections for the decay chain of Fig. 1 for $M_t=50$ GeV for $pp\to D\bar{D}$ at $\sqrt{s}=40$ TeV. The solid line is the total decay rate for the decay chain of Fig. 1. The dotted, short-dash, dot-dash, and long-dash lines are the one-, two-, three-, and four-jet cross sections, respectively.

jet cross sections are also useful for extracting the signal (see Table I).

The multijet cross sections for this scenario with cuts on the p_T of the lepton and on $\mathcal{M}_T(p_l,p_T^{\text{miss}})$,

$$p_{lT} > 30 \text{ GeV}, \quad \mathcal{M}_T(p_l,p_T^{\text{miss}}) > 50 \text{ GeV} , \tag{2.3}$$

are given in Ref. 7. For $M_D = 600$ GeV, the three-jet cross section with these cuts is about 1 pb. Hence the cuts on p_{lT} and $\mathcal{M}_T(p_l,p_T^{\text{miss}})$ reduce the jet cross sections by about a factor of 2.

There are also backgrounds from W pair production and from W plus jet production. Kim[8] investigated the background to the single-lepton signal from $pp \to W^+W^-$ for $M_t = 40$ GeV. He found that by looking for six-jet events, this background could be completely overcome. Similarly, the background from W plus jets can be significantly reduced by looking for multijet events. Baer *et al.*[12] find $\sigma_{4\text{ jet}}(D\bar{D})/\sigma_{W+\text{jets}} \simeq 10$ for $M_D = 240$ GeV for the single lepton signal. Clearly, W plus jets is a significant source of background for $M_D > 200$ GeV. However, the stringent cuts we have applied in total transverse energy ($E_T > 800$ GeV) will further reduce this background. Obviously, it is crucial to be able to extract multijet events in order to overcome the W plus jet background.

There is also an important contribution to both the signal and the top-quark background from the QCD process, $pp \to Q\bar{Q}g$. These contributions are contained in the radiative corrections of Ref. 10 and tend to be largest at low p_T. The combination of a p_T cut and our very severe E_T cut significantly reduces this contribution.

III. ONE-LEPTON SIGNAL ($M_t = 100$ GeV)

In this section we consider $D\bar{D}$ pair production where the final state again consists of one high-p_T lepton and some number of jets. We compare this signal with the background from $t\bar{t}$ production for $M_t = 100$ GeV. Since in this case the t can decay into physical W's, the kinematics are different than in Sec. II. The possible decay chains leading to a single lepton in the final state are shown in Fig. 8 for $D\bar{D}$ and for $t\bar{t}$ production. As in Sec. II we have assumed that the charge of the lepton can be determined and have summed over e and μ production.

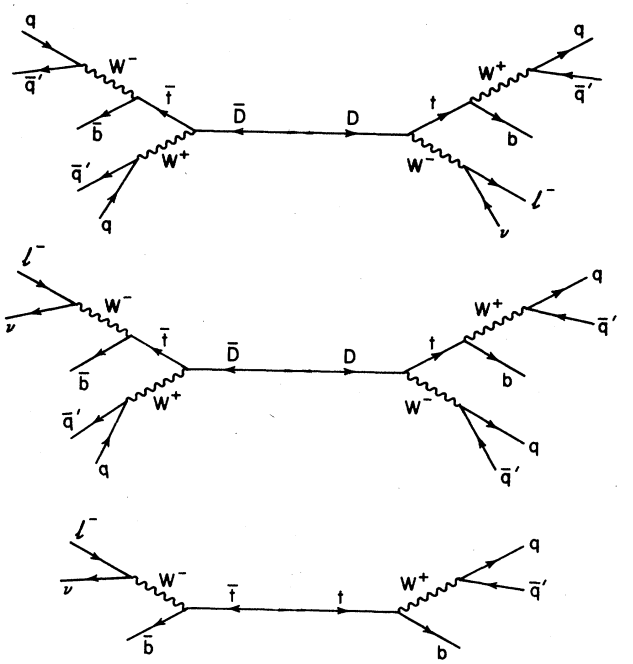

FIG. 8. Decay chains leading to a single lepton in the final state when $M_t = 100$ GeV. Also shown is the background from $t\bar{t}$ production.

The total cross section for this decay chain is shown in Table II for several quark masses. The D-quark production rates are bigger for $M_t = 100$ GeV than for $M_t = 50$ GeV because there are more ways to obtain a single lepton in the final state when $M_t > M_W$.

The p_T distribution of the lepton is shown in Fig. 9 for $M_D = 200$, 400, and 600 GeV and for $M_t = 100$ GeV. The $t\bar{t}$ signal has much the same shape as the D signal. However, the E_T distribution of the $t\bar{t}$ background and the D-quark signal are strikingly different (see Fig. 10). A cut on $E_T > 800$ GeV efficiently rejects the top-quark background while retaining a significant portion of the D quark signal (see Table II). For an integrated luminosity of $10^{40}/\text{cm}^2$, there will be ~ 1600 top-quark events and about 10^5 D-quark events per year for $M_D < 600$ GeV and $E_T > 800$ GeV. As in Sec. II the cross section is rather

TABLE II. $D\bar{D} \to 1$ lepton plus jets ($M_t = 100$ GeV). σ is the cross section for $pp \to D\bar{D} \to l^{\pm}X$ at $\sqrt{s} = 40$ TeV and $l = e$ or μ. σ^{A} has $E_T > 800$ GeV. The column labeled $t\bar{t}$ is the background from $pp \to t\bar{t}$. All cross sections are in nb.

	$M_D = 200$ GeV	$M_D = 400$ GeV	$M_D = 600$ GeV	$t\bar{t}$
σ	0.78	4.0×10^{-2}	6.3×10^{-3}	13.0
σ^{A}	2.3×10^{-2}	1.5×10^{-2}	5.5×10^{-3}	1.6×10^{-4}
$\sigma_{1\text{ jet}}$	1.5×10^{-3}	4.1×10^{-6}	8.3×10^{-7}	5.2
$\sigma^{\text{A}}_{1\text{ jet}}$		1.9×10^{-6}	8.0×10^{-8}	1.9×10^{-5}
$\sigma_{2\text{ jet}}$	1.0×10^{-1}	2.3×10^{-3}	3.9×10^{-4}	6.4
$\sigma^{\text{A}}_{2\text{ jet}}$	1.5×10^{-2}	1.2×10^{-3}	3.4×10^{-4}	1.5×10^{-4}
$\sigma_{3\text{ jet}}$	3.0×10^{-1}	1.5×10^{-2}	3.1×10^{-3}	0.76
$\sigma^{\text{A}}_{3\text{ jet}}$	6.6×10^{-3}	6.5×10^{-3}	2.8×10^{-3}	
$\sigma_{4\text{ jet}}$	2.9×10^{-1}	1.6×10^{-2}	2.2×10^{-3}	1.1×10^{-3}
$\sigma^{\text{A}}_{4\text{ jet}}$	1.0×10^{-3}	5.5×10^{-3}	2.0×10^{-3}	

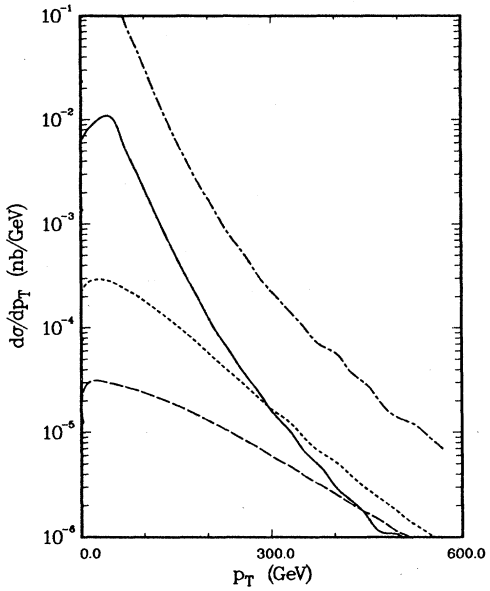

FIG. 9. p_T distribution of the final lepton for the one-lepton decay chain of Fig. 8 for $M_t = 100$ GeV for $pp \to D\bar{D}$ at $\sqrt{s} = 40$ TeV. The dot-dash line is the background from $t\bar{t}$ production and the solid, dotted, and dashed lines are the signal from $D\bar{D}$ production for $M_D = 200$, 400, and 600 GeV, respectively.

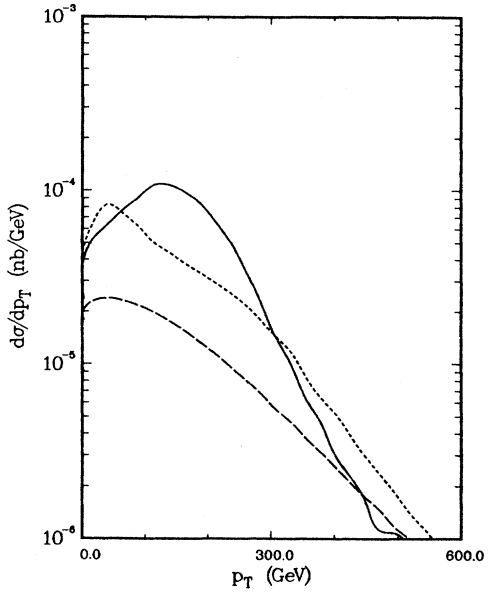

FIG. 11. p_T distribution of the final lepton for the one-lepton decay chain of Fig. 8 with the cut $E_T > 800$ GeV for $M_t = 100$ GeV for $pp \to D\bar{D}$ for $\sqrt{s} = 40$ TeV. The solid, dotted, and dashed lines are the signal from $D\bar{D}$ production $M_D = 200$, 400, and 600 GeV, respectively. Note that the $t\bar{t}$ background has been eliminated by the cut on E_T, $d\sigma/dp_T(E_T > 800$ GeV$) < 10^{-6}$ nb/GeV for top production.

insensitive to the D-quark mass after the cut on E_T is imposed. As shown in Fig. 11, with this stringent cut on E_T the p_T distribution of the lepton is quite flat.

The multijet cross sections are shown in Fig. 12. As before, the four-jet cross section has little background from top quarks. The two-jet cross section with a cut on $E_T > 800$ GeV also can be cleanly separated from the background (see Table III). The multijet cross sections for this scenario with cuts $p_{lT} > 30$ GeV and

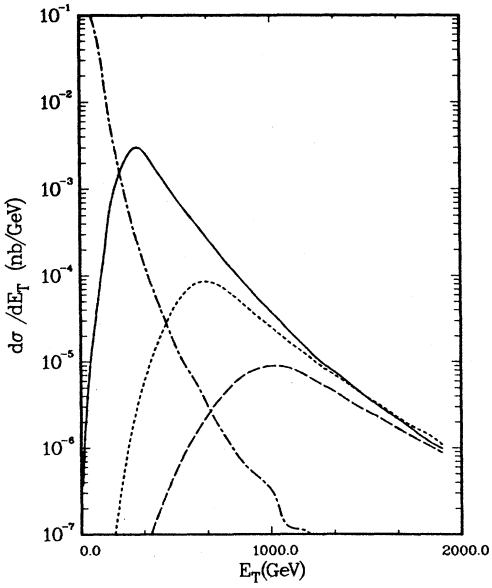

FIG. 10. E_T distribution for the one-lepton decay chain of Fig. 8 for $M_t = 100$ GeV for $pp \to D\bar{D}$ at $\sqrt{s} = 40$ TeV. The dot-dash line is the background from $t\bar{t}$ production and the solid, dotted, and dashed lines are the signal from $D\bar{D}$ production for $M_D = 200$, 400, and 600 GeV, respectively.

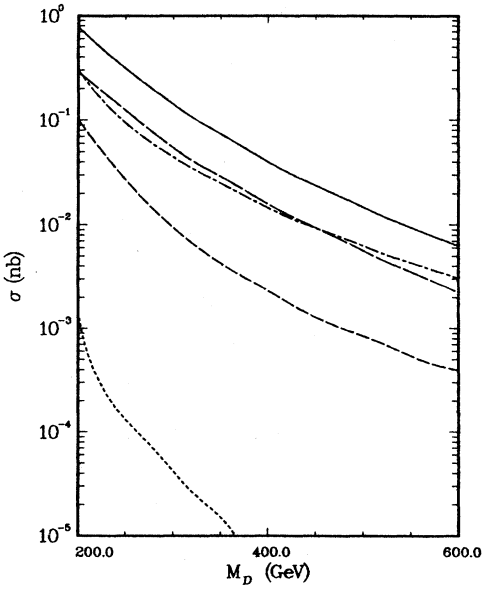

FIG. 12. Multijet cross sections for $pp \to D\bar{D}$ at $\sqrt{s} = 40$ TeV for $M_t = 100$ GeV and the decay chain of Fig. 8. The solid line is the differential decay rate for the decay chain of Fig. 8. The dotted, short-dash, dot-dash, and long-dash lines are the one-, two-, three-, and four-jet cross sections, respectively.

$\mathcal{M}_T(p_l,p_T^{\rm miss})>80$ GeV are given in Ref. 7. With these cuts, the three-jet cross section for $M_D=600$ GeV is slightly larger than 1 pb. This corresponds to about 1000 events per year with an integrated luminosity of $10^{40}/\text{cm}^2$. As in the previous section we see that the cuts on p_{lT} and $\mathcal{M}_T(p_l,p_T^{\rm miss})$ reduce the jet cross sections by about a factor of 2.

IV. TWO-LEPTON SIGNAL ($M_t=50$ GeV)

Here we discuss $D\bar{D}$ pair production with a final state of two high-p_T leptons plus jets for $M_t=50$ GeV. This decay chain has been extensively studied in Ref. 8. The possible decay chains leading to two unlike sign leptons in the final state for $D\bar{D}$ and $t\bar{t}$ production are shown in Fig. 13. Again, we have summed over e and μ production.

The cross sections for the D-quark production and decay into final states with two leptons are smaller than for the one-lepton case because of the additional leptonic broadening ratio. For $M_D=400$ GeV, there will be about 10^5 events per year with a standard integrated luminosity of $10^{40}/\text{cm}^2$ for pp collisions at $\sqrt{s}=40$ TeV.

As in the scenarios with only a single lepton in the final state, an effective kinematic cut is one of the total transverse energy. The E_T distribution for the decay chain of Fig. 13 is shown in Fig. 14. The same cut as in the previous sections, $E_T>800$ GeV, reduces the signal to a level of about 10^{-3} nb, while the $t\bar{t}$ rate with this cut is about

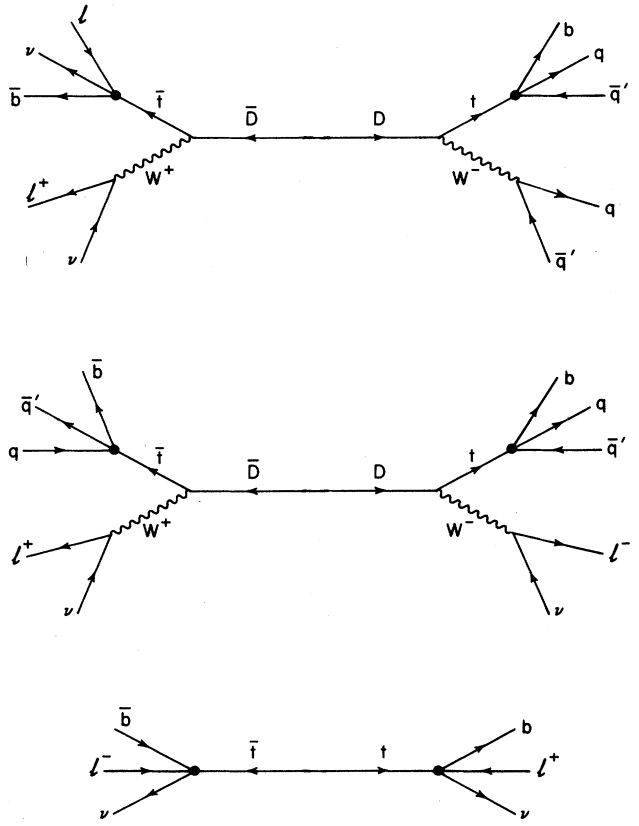

FIG. 13. Decay chains leading to two opposite-sign leptons in the final state when $M_t=50$ GeV. Also shown is the background from $t\bar{t}$ production.

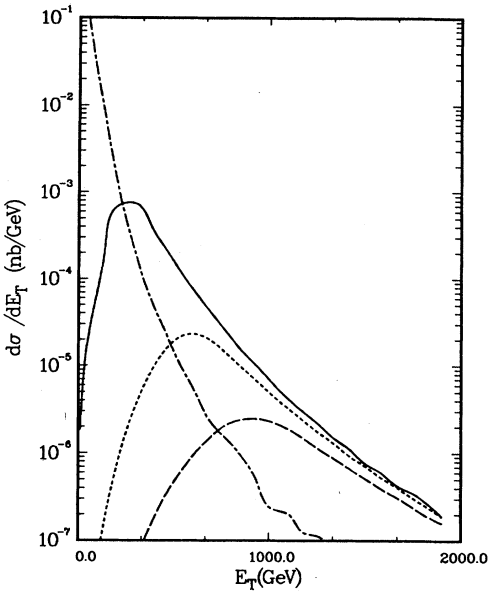

FIG. 14. E_T distribution for the two-lepton decay chain of Fig. 13 for $M_t=50$ GeV for $pp\to D\bar{D}$ at $\sqrt{s}=40$ TeV. The dot-dash line is the background from $t\bar{t}$ production and the solid, dotted, and dashed lines are the signal from $D\bar{D}$ production for $M_D=200$, 400, and 600 GeV, respectively.

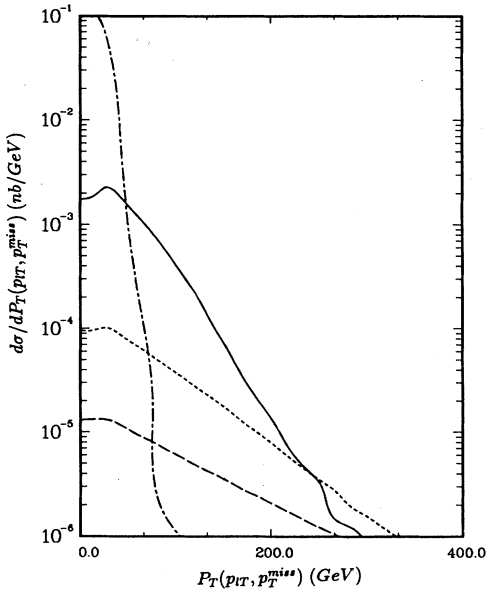

FIG. 15. Transverse momentum between the lepton and the missing transverse momentum $P_T(p_l,p_T^{\rm miss})$ for the two-lepton decay chain of Fig. 13 for $M_t=50$ GeV for $pp\to D\bar{D}$ at $\sqrt{s}=40$ TeV. The dot-dash line is the background from $t\bar{t}$ production and the solid, dotted, and dashed lines are the signal from $D\bar{D}$ production for $M_D=200$, 400, and 600 GeV, respectively.

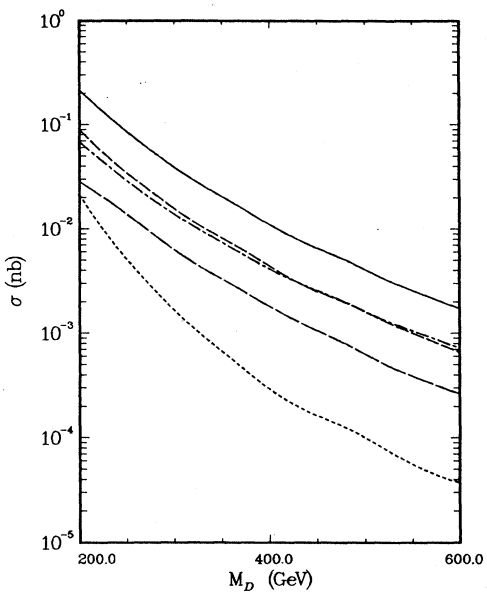

FIG. 16. Multijet cross sections for the two-lepton decay chain of Fig. 13 for $M_t = 50$ GeV for $pp \to D\bar{D}$ at $\sqrt{s} = 40$ TeV. The solid line is the differential decay rate for the decay chain of Fig. 13. The dotted, short-dash, dot-dash, and long-dash lines are the one-, two-, three-, and four-jet cross sections, respectively.

10^{-4} nb. An equally effective cut is that on $P_T(p_l, p_T^{\text{miss}})$, as is seen from Fig. 15. The effects of various cuts are illustrated in Table III.

The multijet plus two-lepton cross sections are shown in Fig. 16. Because the b quark is always assumed to yield a single hadronic jet, the $t\bar{t}$ background can never yield more than two jets plus two leptons if $M_t < M_W$. Hence three or four jets plus two unlike sign leptons are excellent signals for heavy-quark production. Note that the three-jet cross sections for this scenario ($\sigma = 9\times10^{-2}$, 4×10^{-3}, 7×10^{-4} nb for $M_D = 200$, 400, 600 GeV) are larger than those of the one-lepton scenario when the necessary cuts are imposed to extract the lepton plus jet signal from the background.

V. TWO-LEPTON SIGNAL ($M_t = 100$ GeV)

In this section we discuss $D\bar{D}$ pair production with a final state of two unlike sign high-p_T leptons plus jets for $M_t = 100$ GeV. In this case, the top quark can decay into a physical W and the final states are in general quite complicated. The possible decay chains for this scenario are shown in Fig. 17.

For $M_D < 400$ GeV, an effective cut is again one on the total transverse energy, $E_T > 800$ GeV. However, as the quark mass is increased, this cut becomes less effective, as can be seen from Fig. 18. The same is true of the cuts on $\mathcal{M}_T(p_l, p_T^{\text{miss}})$ and $P_T(p_l, p_T^{\text{miss}})$ (see Table IV).

In order to extract the heavy-quark signals for $M_d \simeq 600$ GeV, it is necessary to look at the jet cross sections. The multijet cross sections are shown in Fig. 19. Because of our definition of jets, there is no two-lepton plus three- or four-jet background from top production. This makes the three- and four-jet cross sections excellent signals.

The p_T distribution of the highest-p_T jet is shown in

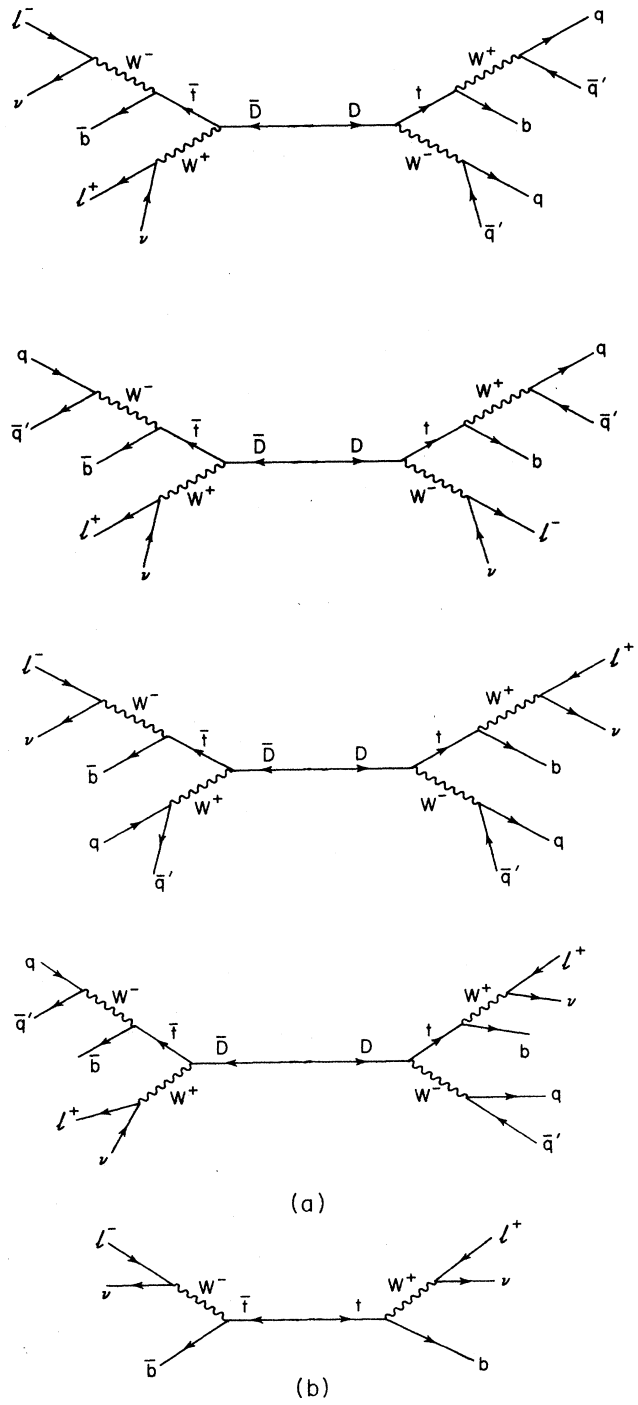

FIG. 17. (a) Decay chains leading to two opposite-sign leptons in the final state when $M_t = 100$ GeV. (b) Background from $t\bar{t}$ production.

TABLE III. $D\bar{D}\to 2$ lepton plus jets ($M_t=50$ GeV). σ is the cross section for $pp\to D\bar{D}\to l^+l'^-X$ at $\sqrt{s}=40$ TeV and $l,l'=e$ or μ. $\sigma^{\rm A}$ has $E_T>800$ GeV, $\sigma^{\rm C}$ has $P_T(p_l,p_T^{\rm miss})>150$ GeV, and $\sigma^{\rm E}$ has both the above cuts. The column labeled $t\bar{t}$ has the background from $pp\to t\bar{t}$. All cross sections are in nb.

	$M_D=200$ GeV	$M_D=400$ GeV	$M_D=600$ GeV	$t\bar{t}$
σ	2.2×10^{-1}	1.1×10^{-2}	1.7×10^{-3}	19.0
$\sigma^{\rm A}$	4.1×10^{-3}	2.8×10^{-3}	1.3×10^{-3}	1.9×10^{-4}
$\sigma^{\rm C}$	1.6×10^{-3}	8.9×10^{-4}	2.8×10^{-4}	3.8×10^{-8}
$\sigma^{\rm E}$	9.8×10^{-5}	2.5×10^{-4}	2.1×10^{-4}	
$\sigma_{1\text{ jet}}$	2.1×10^{-2}	2.9×10^{-4}	3.7×10^{-5}	5.6
$\sigma^{\rm A}_{1\text{ jet}}$	2.2×10^{-4}	3.8×10^{-5}	1.7×10^{-5}	2.8×10^{-5}
$\sigma^{\rm C}_{1\text{ jet}}$	4.6×10^{-4}	5.0×10^{-5}	1.2×10^{-5}	3.8×10^{-8}
$\sigma^{\rm E}_{1\text{ jet}}$	4.1×10^{-6}	4.4×10^{-6}	5.6×10^{-6}	
$\sigma_{2\text{ jet}}$	9.0×10^{-2}	4.4×10^{-3}	6.6×10^{-4}	1.7
$\sigma^{\rm A}_{2\text{ jet}}$	3.2×10^{-3}	9.7×10^{-4}	4.5×10^{-4}	1.7×10^{-4}
$\sigma^{\rm C}_{2\text{ jet}}$	8.1×10^{-4}	4.5×10^{-4}	1.3×10^{-4}	
$\sigma^{\rm E}_{2\text{ jet}}$	7.2×10^{-5}	9.6×10^{-5}	8.2×10^{-5}	
$\sigma_{3\text{ jet}}$	6.9×10^{-2}	4.1×10^{-3}	7.3×10^{-4}	
$\sigma^{\rm A}_{3\text{ jet}}$	6.3×10^{-4}	1.2×10^{-3}	5.9×10^{-4}	
$\sigma^{\rm C}_{3\text{ jet}}$	2.9×10^{-4}	3.0×10^{-4}	1.1×10^{-4}	
$\sigma^{\rm E}_{3\text{ jet}}$	2.2×10^{-5}	1.2×10^{-4}	9.4×10^{-5}	
$\sigma_{4\text{ jet}}$	2.9×10^{-2}	1.8×10^{-3}	2.6×10^{-4}	
$\sigma^{\rm A}_{4\text{ jet}}$	1.9×10^{-5}	4.9×10^{-4}	2.2×10^{-4}	
$\sigma^{\rm C}_{4\text{ jet}}$	1.4×10^{-5}	8.1×10^{-5}	2.5×10^{-5}	
$\sigma^{\rm E}_{4\text{ jet}}$		2.9×10^{-5}	2.1×10^{-5}	

TABLE IV. $D\bar{D}\to 2$ lepton plus jets ($M_t=100$ GeV). σ is the cross section for $pp\to D\bar{D}\to l^+l'^-X$ at $\sqrt{s}=40$ TeV and $l,l'=e$ or μ. $\sigma^{\rm A}$ has $E_T>800$ GeV, $\sigma^{\rm B}$ has $m_T(p_l,p_T^{\rm miss})>50$ GeV, $\sigma^{\rm C}$ has $P_T(p_l,p^{T\,\rm miss})>150$ GeV, and σ^{F} has p_T (fast jet) >300 GeV. The column labeled $t\bar{t}$ has the background from $pp\to t\bar{t}$. All cross sections are in nb.

	$M_D=200$ GeV	$M_D=400$ GeV	$M_D=600$ GeV	$t\bar{t}$
σ	0.26	1.3×10^{-2}	2.1×10^{-3}	2.1
$\sigma^{\rm A}$	1.8×10^{-3}	1.4×10^{-3}	9.1×10^{-4}	1.5×10^{-4}
$\sigma^{\rm B}$	8.4×10^{-3}	3.2×10^{-3}	1.1×10^{-3}	1.4×10^{-3}
$\sigma^{\rm C}$	2.6×10^{-4}	3.7×10^{-4}	1.9×10^{-4}	
$\sigma_{1\text{ jet}}$	1.9×10^{-2}	1.9×10^{-4}	2.6×10^{-5}	3.6×10^{-1}
$\sigma^{\rm A}_{1\text{ jet}}$	1.5×10^{-4}	3.7×10^{-5}	7.8×10^{-6}	3.2×10^{-5}
$\sigma^{\rm B}_{1\text{ jet}}$	2.0×10^{-3}	8.8×10^{-5}	1.9×10^{-5}	3.2×10^{-4}
$\sigma^{\rm C}_{1\text{ jet}}$	7.4×10^{-5}	1.3×10^{-5}	4.4×10^{-6}	
$\sigma^{\rm F}_{1\text{ jet}}$	3.2×10^{-3}	1.2×10^{-4}	2.4×10^{-5}	1.4×10^{-6}
$\sigma_{2\text{ jet}}$	1.0×10^{-1}	4.4×10^{-3}	8.1×10^{-4}	1.2×10^{-1}
$\sigma^{\rm A}_{2\text{ jet}}$	1.5×10^{-3}	6.1×10^{-4}	3.2×10^{-4}	1.2×10^{-4}
$\sigma^{\rm B}_{2\text{ jet}}$	5.3×10^{-3}	1.3×10^{-3}	4.3×10^{-4}	1.1×10^{-3}
$\sigma^{\rm C}_{2\text{ jet}}$	1.5×10^{-4}	1.5×10^{-4}	7.0×10^{-5}	
$\sigma^{\rm F}_{2\text{ jet}}$	7.9×10^{-3}	2.1×10^{-3}	6.5×10^{-4}	3.6×10^{-5}
$\sigma_{3\text{ jet}}$	1.1×10^{-1}	6.0×10^{-3}	9.2×10^{-4}	
$\sigma^{\rm A}_{3\text{ jet}}$	1.1×10^{-4}	5.7×10^{-4}	4.3×10^{-4}	
$\sigma^{\rm B}_{3\text{ jet}}$	1.1×10^{-3}	1.4×10^{-3}	4.8×10^{-4}	
$\sigma^{\rm C}_{3\text{ jet}}$	2.0×10^{-5}	1.7×10^{-4}	9.0×10^{-5}	
$\sigma^{\rm F}_{3\text{ jet}}$	1.4×10^{-3}	1.9×10^{-3}	7.0×10^{-4}	
$\sigma_{4\text{ jet}}$	3.1×10^{-2}	2.4×10^{-3}	3.0×10^{-4}	
$\sigma^{\rm A}_{4\text{ jet}}$		1.4×10^{-4}	1.4×10^{-4}	
$\sigma^{\rm B}_{4\text{ jet}}$	3.5×10^{-5}	3.5×10^{-4}	1.4×10^{-4}	
$\sigma^{\rm C}_{4\text{ jet}}$	1.9×10^{-5}	4.0×10^{-5}	2.4×10^{-5}	
$\sigma^{\rm F}_{4\text{ jet}}$	2.9×10^{-5}	4.6×10^{-4}	1.9×10^{-4}	

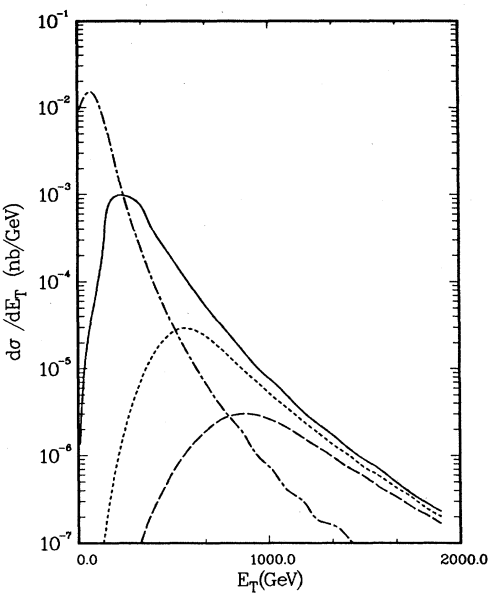

FIG. 18. E_T distribution for the two-lepton decay chain of Fig. 17 for $M_t = 100$ GeV for $pp \to D\bar{D}$ at $\sqrt{s} = 40$ TeV. The dot-dash line is the background from $t\bar{t}$ production and the solid, dotted, and dashed lines are the signal from $D\bar{D}$ production for $M_D = 200$, 400, and 600 GeV, respectively.

Fig. 20. An excellent signal can be found by requiring that there be at least one jet with $p_T^{\text{jet}} > 300$ GeV. As seen in Table IV this cut effectively reduces the top-quark background for all of the multijet cross sections. The jet cross sections with this cut are shown in Fig. 21.

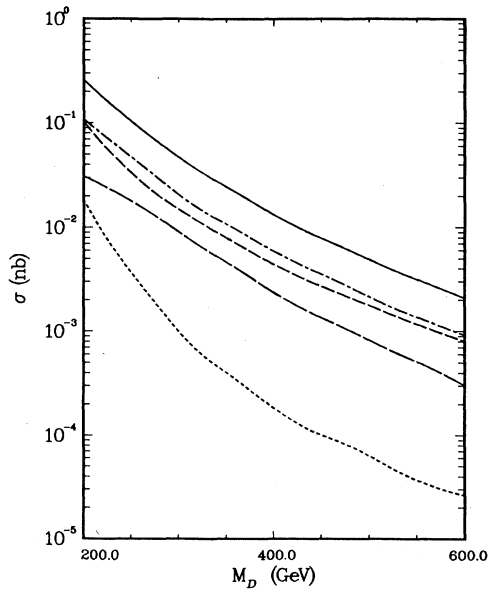

FIG. 19. Multijet cross sections for the decay chain of Fig. 17 for $pp \to D\bar{D}$ at $\sqrt{s} = 40$ TeV for $M_t = 100$ GeV. The solid line is the differential decay rate for the decay chain of Fig. 17. The dotted, short-dash, dot-dash, and long-dash lines are the one-, two-, three-, and four-jet cross sections, respectively.

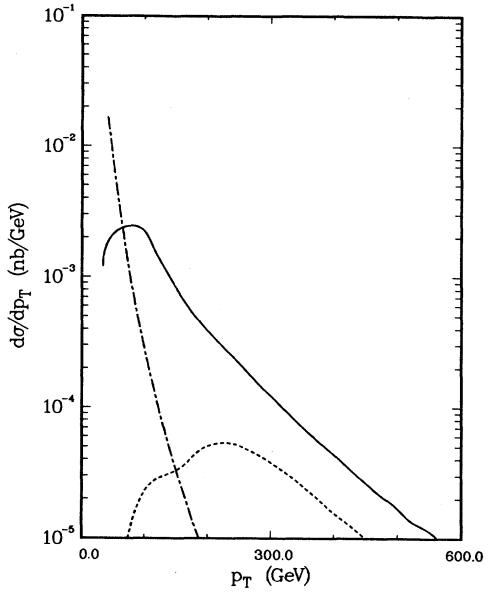

FIG. 20. p_T distribution of the highest-p_T jet for the decay scenario of Fig. 17 for $M_t = 100$ GeV for $pp \to D\bar{D}$ at $\sqrt{s} = 40$ TeV. The dot-dash line is the background from $t\bar{t}$ production and the solid and dotted lines are the signal from $D\bar{D}$ production for $M_D = 200$ and 400 GeV, respectively.

VI. CONCLUSIONS

We have studied the production of a fourth-generation D quark yielding a one- or two-lepton plus multijet signature. We found that the combination of simple kinetic

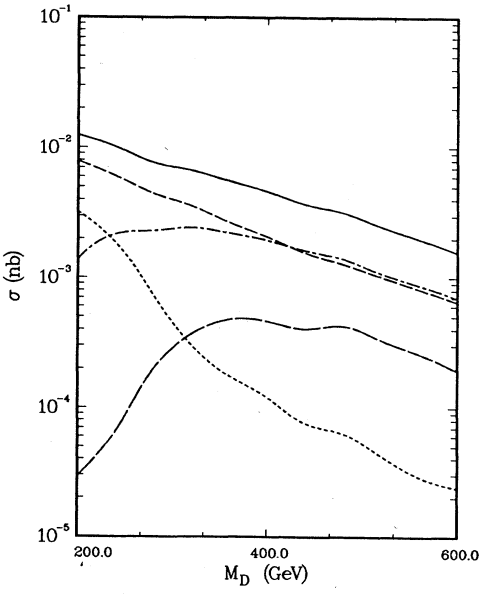

FIG. 21. Multijet cross sections for $pp \to D\bar{D}$ at $\sqrt{s} = 40$ TeV for $M_t = 100$ GeV with at least one jet with $p_T^{\text{jet}} > 300$ GeV. The solid line is the differential decay rate for the decay chain of Fig. 17 and the dotted, short-dash, dot-dash, and long-dash lines are the one-, two-, three-, and four-jet cross sections, respectively.

cuts with three- and four-jet signals is sufficient in each case to eliminate the background from top production. In particular, we found that the transverse energy E_T is a very useful kinematic variable for separating the signal and background. Clearly for this approach to succeed, it is crucial to be able to find multijet events.

In our crude analysis we were able to extract the D-quark signal from the top-quark background for D-quark masses up to 600 GeV with several thousand events per year remaining after the necessary cuts were made. With a more sophisticated analysis, it will undoubtably be possible to go to higher masses.

In principle, the heavy-quark mass could be reconstructed by picking out events with a single isolated hard lepton, then considering the jets in the opposite hemisphere and forming an invariant mass from the jet four-vector. Preliminary results using a parton-level Monte Carlo simulation indicate that this procedure results in a very distinctive signal in the jet invariant mass for all quark masses we have considered. This crude procedure indicates that good jet reconstruction is likely to be very important in extracting physics at the SSC (Ref. 6) (which included the effects of hadronization) was able to reconstruct the heavy-quark mass for $M_D = 500$ GeV in the two-lepton-decay scenario by looking at W^+W^- invariant masses for events with more than four jets. Similar results were obtained in Ref. 12.

In summary, by looking for multijet events with high-p_T leptons, the SSC should be able to find signals for heavy-quark production up to masses on the order of 600 GeV.

ACKNOWLEDGMENTS

This work was supported in part by the Natural Science and Engineering Research Council of Canada and under Contract No. DE-AC02-76CH00016 with the U.S. Department of Energy. S.G. gratefully acknowledges Jim Davis for the use of his micro-VAX computer.

[1]For an overview of hadron collider physics see, for example, E. Eichten *et al.*, Rev. Mod. Phys. **56**, 579 (1984).

[2]U. Amaldi *et al.*, Phys. Rev. D **36**, 1385 (1987).

[3]W. Marciano, in Proceedings of the First International Symposium on the Fourth Family of Quarks and Leptons, Santa Monica, California, 1987, edited by D. Cline and A. Soni (to be published).

[4]M. Chanowitz, M. Furman, and I. Hinchcliffe, Nucl. Phys. **B153**, 402 (1979).

[5]A top quark satisfying the bound of Eq. (1.1) will presumably be found at the Fermilab Collider. See, for example, H. Baer, V. Barger, H. Goldberg, and R. J. N. Phillips, Phys. Rev. D **37**, 3152 (1988); D. Atwood, A. P. Contogouris, and H. Tanaka, *ibid.* **36**, 1547 (1987).

[6]S. Dawson, J. Haggerty, S. Protopopescu, and P. Sheldon, in *Proceedings of the Workshop on Experiments, Detectors, and Experimental Areas for the SSC,* Berkeley, CA, edited by R. Donaldson and M. Gilchriese (World Scientific, Singapore, 1988).

[7]S. Dawson and S. Godfrey, in *Proceedings of the Workshop on Experiments, Detectors, and Experimental Areas for the SSC* (Ref. 6).

[8]V. Barger *et al.* Phys. Rev. D **30**, 947 (1984); B. Cox, F. Gilman, and T. Gottschalk, in *Physics of the Superconducting Super Collider,* proceedings of the Summer Study, Snowmass, Colorado, 1986, edited by R. Donaldson and J. Marx (Division of Particles and Fields of the APS, New York, 1987), p. 33; E. Glover and D. Morris, *ibid.* p. 238; S. Kim, *ibid.* p. 241; H. Baer, V. Barger, and H. Goldberg, Phys. Rev. Lett. **59**, 860 (1987); H. Baer, in *Proceedings of the Workshop on Experiments, Detectors, and Experimental Areas for the SSC* (Ref. 6); Z. Kunszt, in *Proceedings of the Workshop on Physics of Future Accelerators,* La Thiule, Italy, 1987, edited by J. H. Mulvey (CERN Report No. 87-07, Geneva, Switzerland, 1987).

[9]M. Gluck, J. F. Owens, and E. Reya, Phys. Rev. D **17**, 2324 (1978); B. L. Combridge, Nucl. Phys. **B151**, 429 (1979); J. Babcock, D. Sivers, and S. Wolfram, Phys. Rev. D **18**, 162 (1978); K. Hagiwara and T. Yoshino, Phys. Lett. **80B**, 282 (1979); L. M. Jones and H. Wyld, Phys. Rev. D **17**, 178 (1978); H. Georgi *et al.*, Ann. Phys. (N.Y.) **114**, 173 (1978).

[10]P. Nason, S. Dawson, and R. K. Ellis, Nucl. Phys. **B303**, 607 (1988).

[11]F.E. Paige and S. D. Protopopescu, in *Physics of the Superconducting Super Collider* (Ref. 8), p. 320.

[12]H. Baer, V. Barger, H. Goldberg, and J. Ohnemus, Phys. Rev. D **38**, 2222 (1988).